Desalination and Water Treatment
www.deswater.com
doi: 10.5004/dwt.2019.24709

169 (2019) 395–411
November

A green 3D scaffolds based on chitosan with thiol group as a model for adsorption of hazardous organic dye pollutants

Fernanda G.L. Medeiros Borsagli

Universidade Federal dos Vales do Jequitinhonha e Mucuri (UFVJM), Av. 01, 1150 Cidade Universitária, Zip code 39440-039, Janaúba-MG, Brazil, Tel. +55 38 38293100; Fax: +55 38 38293100; email: fernanda.borsagli@ufvjm.edu.br

Received 17 March 2019; Accepted 23 July 2019

ABSTRACT

Water contamination is an increasing global concern due to deterioration of water quality. Chitosan and its derivatives are one of the most promising and applicable bio-sorbents for dye adsorption. This study investigated the adsorption properties of novel 3D scaffolds prepared with chitosan using modifiers with thiol group (or thiomers) for wastewater treatment. These thiomers were produced by the covalent conjugation of thiol moieties (cysteine) to chitosan (ChiCys), mediated by a zero-length crosslinker. Porous 3D scaffolds were tested for methyl orange and methylene blue adsorption. The results demonstrated high thiolation (ChiCys = 500 ± 39 μmol g^{-1}). The prepared scaffolds showed a hierarchal interconnected 3D porous structure and chemical stability suitable for use as bio-sorbents. Moreover, they presented cytocompatibility using in vitro bioassays. These scaffolds demonstrated high adsorption efficiency (over 90%) and maximum uptake (305 ± 2 mg g^{-1}) at pH = 7.0 for methyl orange (100 mg L^{-1}). The adsorption was well fitted to a pseudo-second-order kinetics and Langmuir equations. Thus, for the first time, thiomer 3D-scaffolds were produced by combining green bio-sorbent behavior for organic dyes, which offers an innovative strategy for the treatment of contaminated water bodies.

Keywords: Adsorption; Bio-sorbent; Thiomers; Scaffold sorbent; Wastewater treatment

1. Introduction

Water availability for economic development and conservation of life is a theme of great concern, because of the increasing occurrence of vents related to climate change combined with the deterioration of water quality due to anthropogenic contamination [1]. Among these, pollutants such as dyes, phenolics, pharmaceutics and pesticides have been recently a cause of concern, as they showed an extreme toxicity and persistence in the environment. Although chemical and biological treatments are available for the removal of some organic compounds, by-products produced by their degradation can also be harmful [2–4]. In that sense, hazardous organic dyes, which are released from textile, paint, paper, varnishes, ink, plastics, pulp, cosmetics, tannery and plastic, are one of the key causes of water pollution [5,6].

The industrial effluents from different sources are a significant cause of water pollution. These pollutants present a great visibility even at very low concentrations. Moreover, they show a recalcitrance nature, which gives an undesirable color to the water, reducing sunlight penetration, resisting photochemical and biological attack. In addition, their degradation products are toxic, mutagenic and carcinogenic [5]. Nowadays, around 15% of different dyes are present in the effluent. Furthermore, approximately 10,000 different types of pigments and over 700,000 tons are produced worldwide annually [4,6–8].

Normally, the effluents are usually treated by chemical precipitation, membrane separation, evaporation, electrolysis, among other processes. Therefore, some methods are ineffective, present a relatively high cost, involve difficult of operation, have complicated design, and most of them present shortcomings, high maintenance costs, generation of toxic sludge and complicated procedure involved in the treatment [9–11]. For this reason, selective wastewater treatment process for the capture/immobilization of specific dyes and its regeneration is needed. The adsorption process is competitive and cost-efficient for the treatment of effluents [12]. In fact, adsorption processes are one of the most successful techniques for color removal from wastewater among all the techniques developed so far [1,4]. In this way, a large variety of low-cost adsorbents have been examined for their ability to remove various types of pollutants from water. New effective substitutes based on natural polymers and derivatives such as starch, cellulose, chitosan and lignin have significantly increased considering the concept of economy and environmental friendliness. Moreover, these materials have been observed to desorb faster than activated carbon [4,7,12,13].

The natural polymers are scientifically and industrially attractive, as they present hydrophilic networks with functional groups for developing chemical interactions, which may interact with metallic ions and organic compounds [14,15]. In this sense, there exists an attractive class of soft materials that has been developed based on polyelectrolytes forming hydrogel networks that swell in water instead of dissolving in it. Moreover, they can retain extremely large amounts of aqueous medium relative to their own mass [4]. This behavior is caused by chemical interactions, which enables hydrogen bonding between water molecules and functional groups of the polymer network, leading to water absorption from 10 to 100 times its weight and this allows its use broadly in a variety of applications [4,15]. In addition, some of these natural polymers, such as chitosan, have potential for antimicrobial activity, and these microorganism are very resistant and are presented in the effluents [16–18].

In this context, thiolated chitosan has many predominant features such as the improved chemical stability based on the disulfide forming covalent bonds, and characteristics that involve electrostatic interaction [19,20]. Thus, there is a vast field to be exploited based on the combination of chemical functionalities with the chitosan (Chi) polysaccharide backbone producing a new class of thiolated chitosan polymers such as thiolated chitosan with cysteine for numerous applications [21–23]. Therefore, it is essential to combine all the mentioned features of chitosan and thiomers into a single design to address the different aspects of a dynamic adsorption process.

Chitosan (CH) is a polysaccharide that is obtained by the deacetylation of chitin. This chitin is abundantly available in nature, as it is presented in many invertebrates and in the cell wall of most algae and fungi [24]. Chitosan and derivatives have been widely investigated as bio-sorbents for water treatment mostly in the removal of heavy metals and dyes [25–27]. On this wise, the chemical conjugation process of chitosan with thiol-bearing ligands produces thiomers with a high level of many properties [28]. However, there are some reports in the literature about the fundamentals of sulfur modification of chitosan in relation to metal adsorption capacity. In these works, most of them describe the adsorption of heavy metals [29–31]. Nevertheless, these chitosan modifications with sulfur groups, as thiol, increase the stability of complexed 'soft acids', thus enhancing sorption capacity as well as selectivity [29–31]. Despite the numerous investigations on improved functional characteristics and applications, to the best of the author's knowledge, the relationship between thiolated chitosans and pigments has not been mentioned in the literature.

In this sense, further investigations on the effect of thiolated chitosan on the adsorption of pigments are required. Thus, this study reports a facile green synthesis of novel soft 3D scaffold adsorbents based on thiolated chitosans (chitosan using cysteine). This research evaluated the influence of the chemical functionalization on the adsorption of hazardous organic dyes, including the kinetics, isotherms, pH and mechanisms involved, thus supporting prospective use of these scaffolds as an alternative and ecologically sustainable proposal for wastewater treatment.

2. Experimental section

2.1. Materials

All the reagents and precursors were used as received. These included sodium hydroxide (Sigma-Aldrich, USA, ≥99%, NaOH), hydrochloric acid (Sigma-Aldrich, USA, 36.5%–38.0%, HCl), acetic acid (Synth, Brazil, 99.8%, MM = 60.05 g mol^{-1}, CH_3CO_2H), L-Cysteine (Sigma-Aldrich, USA, $HSCH_2CH(NH_2)CO_2H$, MM = 121.16 g mol^{-1}), Ellman's reagent (Sigma-Aldrich, USA, DTNB, 5,5′-dithiobis(2-nitrobenzoic acid), MM = 396.35 g mol^{-1}, $[-SC_6H_3(NO_2)CO_2H]_2$), *N*-(3-dimethylaminopropyl)-*N*′-ethylcarbodiimide hydrochloride – EDC (Sigma-Aldrich, USA, $C_8H_{17}N_3{\cdot}HCl$, MM = 191.7 g mol^{-1}), *N*-hydroxysulfosuccinimide sodium salt – sulfo-NHS (Sigma-Aldrich, USA, ≥98%, $C_4H_4NNaO_6S$, MM = 217.13 g mol^{-1}), sodium phosphate dibasic (Sigma-Aldrich, USA, ≥99.0%, MM = 141.96 g mol^{-1}, Na_2HPO_4), potassium phosphate monobasic (Sigma-Aldrich, USA, ≥99.0%, MM = 136.09 g mol^{-1}, KH_2PO_4), potassium chloride (Sigma-Aldrich, USA, ≥99.0%, MM = 74.55 g mol^{-1}, KCl), sodium chloride (Sigma-Aldrich, USA, ≥99.0%, MM = 58.44 g mol^{-1}, NaCl), ethylenediaminetetraacetic acid (EDTA, Synth, Brazil, $(HO_2CCH_2)_2NCH_2CH_2N(CH_2CO_2H)_2$, >99.99%, MM = 292.24 g mol^{-1}), nitric acid (HNO_3, Sigma-Aldrich, USA, ≥90%, MM = 63.01 g mol^{-1}), methylene blue (MB, Synth, Brazil, $C_{16}H_{18}N_3SCl{\cdot}3H_2O$) and methyl orange (MO, Synth, Brazil, $C_{14}H_{14}N_3NaO_3S$). High-molecular-mass chitosan powder (CHI, molar mass, MM = 310.000 > 375.000 g mol^{-1}, deacetylation degree (DD) ≥75.0%, and viscosity 800–2,000 cP, at 1% in 1% acetic acid, Sigma-Aldrich, USA) was used for polymer modification. Deionized water (Simplicity™, Millipore, Massachusetts, USA) with a resistivity of 18 MW cm was used to prepare all solutions. All preparations and syntheses were performed at room temperature (RT, 25°C ± 2°C) unless otherwise specified.

2.2. Incorporation of thiol group in chitosan with cysteine (ChiCys)

The synthesis of chitosan with cysteine (Cys) was performed according to the molar ratio of reagents 1:2:2 (Chi:EDC:Cys). The synthesis of ChiCys was adapted from

the process reported in the literature [22]. In this sense, 500 mg of chitosan powder was used dissolving in 30 mL of 2% (v/v) acetic acid aqueous solution overnight. In the sequence, 0.7 g of cysteine powder added in 20 mL of phosphate-buffered saline (PBS) solution with 1.2 g of *N*-(3-dimethylaminopropyl)-*N*′-ethylcarbodiimide hydrochloride (EDC) and 0.32 g of *N*-hydroxysulfosuccinimide sodium salt (sulfo-NHS) were maintained under moderate stirring for 1 h at room temperature. Then, this solution was added to chitosan/acetic acid solution and the pH was adjusted to 5.0 ± 0.5 (NaOH, 1.0 mol L^{-1}), because it is needed a major number of de-protonated amino groups to conjugate with carboxylic group at Cys and at elevated pH (pH > 6.0) the thiol group may suffer oxidation process [19,22]. The reaction was performed at room temperature under moderate stirring for 5 h in the darkness. Next, the mixture was dialyzed in the darkness against distilled water using a membrane (12–14 kDa, Sigma-Aldrich, USA) for 7 d at room temperature. The 3D scaffolds were obtained by a freeze-drying process (ModulyoD, Thermo Electron Corporation, Waltham, Massachusetts, USA) at –50°C and 350 ± 50 μbar for approximately 72 h, until the samples reached a constant mass, using the previously prepared solutions (ChiCys). The ChiCys scaffolds were produced with a foam-like aspect and stored at 4°C ± 2°C until further use.

2.3. Thiol polymer characterization

2.3.1. Determination of thiol group content

The determination of the total amount of thiol groups in the ChiCys chain was performed using the Ellman's reagent protocol as reported previously in the literature [19], because a solution of this compound produces a measurable yellow-colored product when it reacts with sulfhydryls, so this reagent (DTNB, 5,5′-dithiobis(2-nitrobenzoic acid)) is very useful as a sulfhydryl assay reagent because of its specificity for –SH groups at neutral pH, high molar extinction coefficient and short reaction time [19]. The amount of total thiol groups was calculated from a calibration curve of cysteine, because sulfhydryl groups may be estimated in a sample by comparison with a standard curve composed of known concentrations of a sulfhydryl-containing compound such as cysteine or other sulfhydryl-containing compound [20], in a concentration range of 1,600–20 μM prepared in the same way as the samples (Fig. S1). All experiments were conducted in triplicate (n = 3), unless specifically noted.

2.3.2. Statistical analysis

All experiments were averaged and statistical analysis was performed using ANOVA (one way included Tukey's test, $p < 0.05$, software Origin v.8.1, OriginLab Corporation, USA) unless specifically noted.

2.3.3. Spectroscopic characterization of samples

Fourier transform infrared spectroscopy (FTIR) spectra were obtained using the attenuated total reflectance method for all samples (ATR, ZnSe crystal prism, 4,000–650 cm^{-1} with 32 scans and a 4 cm^{-1} resolution – Nicolet 6700, Thermo Fisher, Waltham, Massachusetts, USA). All of the experiments were conducted in triplicate (n = 3), unless specifically noted.

Raman spectroscopy was performed with a LabRAM-HR 800 (Horiba Jobin Yvon, Japan) equipped with an Olympus BX-41 microscope provided with lenses of 10×, 50× and 100× and an additional macro lens of 40 mm for all samples. Excitation at 632.8 nm from a helium–neon laser was focused on a spot of 1–2 μm^2 on the samples. The collected back-scattered light was dispersed by a monochromator and detected by an LN_2 (liquid nitrogen)-cooled CCD (charge-coupled device) system. The spectra ranged from 200 to 3,300 cm^{-1} with a step size of 1.1 cm^{-1}. Depending on the background fluorescence, the acquisition time was set from approximately 60–300 s, with a minimum of 10 replicates to increase the signal-to-noise ratio.

^{1}H-NMR (proton nuclear magnetic resonance) spectra of CHI, ChiCys and CHIMerc samples were recorded at 50°C in D_2O/DCl using a Bruker-400 MHz Varian spectrometer (Massachusetts, USA) (90° pulse and 16 scans).

2.3.4. Swelling degree and gel fraction of 3D scaffolds

The swelling degree (SD) of all samples was evaluated in deionized water (pH = 5.5 ± 0.5) as described in the literature [22]. This process was repeated for different time intervals 1, 2, 3, 4, 6, 8 and 24 h to assess the swelling degree until reaching the equilibrium for the hydrogels. The chemical stability in vitro in aqueous solution (referred to as the gel fraction, GF) of ChiCys samples was assessed by measuring the GF. This process was repeated for different time intervals (1, 2, 3, 4, 6, 8 and 24 h) as described in the literature [23]. These experiments were performed with 21 samples for each system (n = 21, 7 samples of 3 different synthesis). The drying procedure for scaffold was using an oven for 24 h at 40°C ± 2°C. This process was used just because the process is accelerated without alterations on the chemical characteristics of the hydrogels. In order to validate these findings, a similar procedure was performed at room temperature 25°C ± 2°C (i.e., without heating at 40°C ± 2°C in an oven) for 24 h (n = 9 replicates) and using the freeze-drying process after the swelling. The results were statistically equivalent (ANOVA, one way included Tukey's test, $p < 0.05$, software Origin v.8.1, OriginLab Corporation, USA).

2.3.5. Morphological analysis of 3D scaffolds

The morphologies of the scaffolds were evaluated using a scanning electron microscope (SEM, FEI-FEG-FIB-QUANTA 3D) coupled with energy dispersion X-ray spectroscopy (EDX, EDAX Bruker, Massachusetts, USA), resolution 0.8 nm. Before examination, the samples were coated with a thin carbon film via sputtering using a low deposition rate, cooling the substrate, and ensuring the maximum distance between the target and the sample to avoid sample damage, the film formed had 30 nm. Images of secondary electrons (SE) and were obtained using an accelerating voltage of 15 kV for all samples at two different planes (transversal and superficial). SEM images were collected and the pore size was estimated based on at least 50 random measurements using the open source image processing program (ImageJ v.1.50+, National Institutes of Health, NIH).

The three-dimensional structures of the scaffolds were investigated using 3D microtomography (SkyScan 1174, Bruker micro-CT, Massachusetts, USA) at a resolution of 12.18 μm, at 40 kV voltage, 100 μA current, 0.7° rotation step, and no filter. Images were reconstructed using NRecon Reconstruction software (v.1.6.1.18, Bruker micro-CT, Massachusetts, USA). CTAn software (v.1.15.4.0, Bruker micro-CT, Massachusetts, USA) was used to analyze the micro-CT datasets in 2D and 3D for morphometry and densitometry, and CTVol software (v. 2.3.1.0, Bruker micro-CT, Massachusetts, USA) was used for 3D visualization of the scaffolds.

As the specific surface area was made by the BET (Brunauer–Emmett–Teller) – Multipoint method using a nitrogen gas sorption analyzer NOVA 1000 Quantachrome. Prior to measurement, the samples were weighed, degassed by placing them into a glass cell under vacuum for at least 120 h at 40°C and weighed again. The BET analyzer's Dewar flask was filled with liquid nitrogen and set into place for analysis of the degassed samples.

2.3.6. Cytotoxicity assay by the (3-(4,5-dimethylthiazol-2-yl)-2,5-diphenyltetrazolium bromide) assay

The kidney cell line of human embryo (HEK 293 T) was kindly provided by Prof. Goes of the Department of Immunology and Biochemistry, UFMG. The cells were cultured in Dulbecco's modified eagle medium (DMEM) with 10% fetal bovine serum, penicillin G sodium (10 units mL^{-1}), streptomycin sulfate (10 mg mL^{-1}), and 25 μg mL^{-1} amphotericin-b (all from Gibco BRL, NY, USA) in a humidified atmosphere of 5% CO_2 at 37°C. The cells were used for the experiments at passage twelve. All of the biological tests were conducted according to ISO standards 10993-5:1999 (Biological evaluation of medical devices; Part 5: tests for in vitro cytotoxicity). HEK 293 T cells were plated (3×10^4 cells) on each sample material. The plates were subjected to UV radiation for 60 min in a sterile flow and washed quickly in ice-cold PBS. The samples were sterilized by UV radiation for 60 min in a sterile flow. Controls were created using cells and DMEM medium (10%); Triton x-100 (1%; Sigma-Aldrich, St. Louis, MO, USA) was used as a positive control, and chips of sterile polypropylene (1 mg mL^{-1}; Eppendorf, Hamburg, Germany) were used as a negative control. After 24 h, all media was aspirated and replaced with 210 μL of culture medium with serum. MTT (170 μL, 5 mg mL^{-1}; Sigma-Aldrich, St. Louis, MO, USA) was added to each well and incubated for 4 h followed by incubation for 16 h with SDS/4% HCl. Subsequently, 100 μL was removed from each well and transferred to a 96-well plane, and the absorbance was quantified using a Varioskan Reader (Thermo Scientific) with a 595 nm filter. The absorbance values were expressed as the percentage of viable cells using Eq. (1). The values of the controls (wells with cells, and no samples) were set to 100% cell viability. All of the experiments were performed with six samples for each system ($n = 6$).

$$\text{Cell viability}(\%) = \left(\frac{\text{Abs of sample and cells}}{\text{Abs of control}}\right) \times 100 \quad (1)$$

2.4. Adsorption and desorption of organic dye pollutants

The adsorption of organic dye pollutants was made using methylene blue (MB) and methyl orange (MO) as model cationic and anionic pigments in water, respectively. MO or MB solutions were prepared from a stock solution of 100 mg L^{-1} in deionized water. The MO and MB solutions were prepared with the concentration 20 mg L^{-1}. Adsorption experiments were conducted by adding approximately 13 mg of the scaffolds (on a dry mass basis) into 5 mL of each MO or MB solution. The experiments were performed at constant pH = 7.0 ± 0.5 and temperature of 23°C ± 2°C in a dark chamber. The adsorption efficiency and adsorption capacity were determined according to literature [25]. The correlation of the absorbance with the dye concentration was performed at the characteristic maximum absorption wavelength of MO (i.e., λ = 465 nm) or MB (i.e., λ = 664 nm) by the standard working curve (Figs. S2a and b) using UV–vis spectroscopy (Lambda EZ-210, PerkinElmer, Massachusetts, USA) in all experiments. Appropriate dilution was performed to ensure that the concentration of the solution was within the range of the standard working curve. The pure chitosan was tested too. Nevertheless, the pure chitosan did not show stability, after 4 h it solubilising completely.

Adsorption kinetic experiments were performed to determine the time for equilibrium for the pigment adsorption (at 20 mg L^{-1}). At increasing time intervals up to 1,440 min (i.e., 24 h, when the equilibrium was reached), the pseudo-first-order, pseudo-second-order and intraparticle diffusion models, were performed according to literature [26] to determine the best kinetic model.

As a preliminary assessment of regeneration of ChiCys, desorption experiments were performed. After adsorption of MO and MB (at 20 mg L^{-1} after 24 h), saturated dye-loaded sorbents were immersed in aqueous KCl solution (3 mol L^{-1}, ionic strength = 1.5), HNO_3 solution (pH = 4.0 ± 0.5), NaOH solution (pH = 10.0 ± 0.5) and EDTA (1 M, pH = 4.5 ± 0.5) to evaluate desorption due to the ion exchange, pH variation and extraction by a complexant, respectively. After 2 h of ultrasonication, the final MO and MB concentrations in solution were analyzed and compared with the amount of dye previously adsorbed. The regeneration of the adsorbent was sequentially operated three times in this way. The efficiency of regeneration was calculated according to the literature [6]. Moreover, the Raman spectroscopy was used to confirm and study the desorption of MO after each cycle.

3. Results and discussion

3.1. Characterization of 3D scaffolds

3.1.1. Analysis of synthesis and determination of total thiol group

After 3 d of lyophilization, the samples seemed as a white foam with spongy structure. This foam (scaffold) showed approximately 0.5 mm of diameter, and 25 mm of length. In this sense, the thiol group attached the primary amino group at the 2nd position of the glucosamine subunits of chitosan, for the immobilization. The carboxylic group of cysteine linked with primary amino group of chitosan via a covalent amide bond formation, this reaction is mediated by a water-soluble ethylcarbodiimide (EDC) as schematically depicted in Fig. 1a. According to the literature [25], the best results for the thiol chitosan with cysteine were found when the molar ratio between Cys:EDC and Cys:Chi was 1:2. Therefore, the molar ratio between

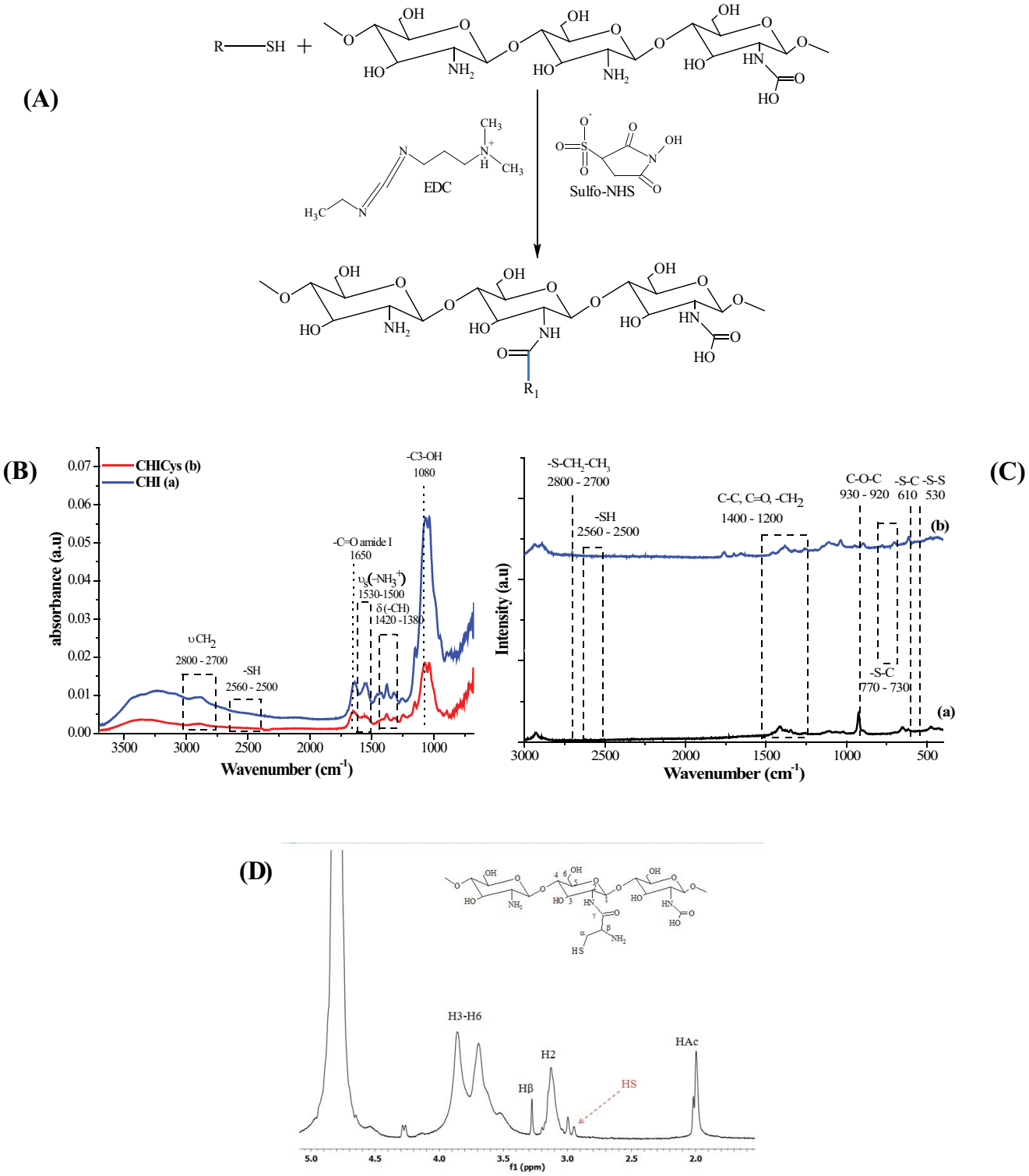

Fig. 1. (A) Schematic representation of chemical functionalization of chitosan with thiol precursors, (B) FTIR of samples Chi (black line), ChiCys (red line), (C) Raman spectra of samples (a) Chi and (b) ChiCys and (D) H^1 NMR spectra of ChiCys.

Cys:EDC significantly influenced the thiol group amount per gram of polymer [28]. However, the solution medium has influenced the functionalization [22]. Nevertheless, some solvents used in the literature present a degree of toxicity, considering that, in this study, the PBS buffer solution was used, as this is the best solvent for sulfo-NHS and EDC, and it is not toxic. The amount of thiol groups on the chitosan-based thiomers determined via Ellman's reagent [19] was 500 ± 39 μmol g^{-1}. The degree of substitution of thiol groups in this study was relatively higher than others found

in the literature [22,28,32,33]. Probably, a more effective thiolation process assigned to distinct optimized experimental conditions, such as the use of sulfo-NHS combined with EDC as a zero-length coupling agent, the buffer solution and solvent (i.e., PBS solution), temperature, pH, concentration of reagents, time of reaction, degree of deacetylation, molar mass of chitosan and others was responsible. Moreover, the high concentration of thiol groups found in this research may improve the properties of pristine chitosan for many potential applications [19,33,34].

3.1.2. Analysis of Raman, FTIR and NMR spectra

The differences observed by comparing the IR spectra can be associated with the functionalization by the thiol precursor with the primary amine in the chitosan glucosamine units. The typical bands of Chi are identified in the FTIR spectra (Fig. 1b): the broad OH and NH stretching bands at 3,450 cm^{-1}; the C–H stretching bands between 2,800 and 2,900 cm^{-1}; the $–CH_2$ bending at 1,420 cm^{-1}; the amide I bands at ~1,655 cm^{-1}; the amide II band at 1,560 cm^{-1}; the amide III band at 1,315–1,320 cm^{-1}; the bands assigned to C–O stretching at 1,030 and 1,075 cm^{-1}; and the band at 897 cm^{-1}, related to the C–O–C glycosidic linkage [28,35]. As cysteine is a heavier group, in the ChiCys spectra is observed, the C–N (1,250–1,320 cm^{-1}) and NH (~1,550 cm^{-1}) bands shifted towards lower frequencies, because of the amide bond formation [35]. Moreover, the formation of amide groups also increases the amide I band due to the augmentation of C=O stretching vibrations. Furthermore, there is an insertion of CH_2 groups in the chitosan polymer structure. Therefore, the insertion of thiol group in the chain of chitosan in this study was qualitatively confirmed by the increase in bands related to CH_2 vibrations at approximately 2,900 and 1,420 cm^{-1}.

The thiol group is very difficult to detect in the FTIR analysis. Then, the Raman spectroscopy was used for the characterization of the thiomers. The typical chitosan bands (Fig. 1c) can be identified in the 3D scaffolds: the amide I bands at ~1,696 cm^{-1}; the amide III band at 1,297 cm^{-1}; the $–CH_2$ bending at ~1,410 cm^{-1}; the bands assigned to C–O stretching at 890 and 920 cm^{-1}; C–H stretching bands between 2,800 and 2,900 cm^{-1}. In addition, the 3D scaffolds presented the bands related to sulfur groups at 610 cm^{-1} (–S–C–) (not highlighted), 540 cm^{-1} (S–S) and 2,560–2,500 cm^{-1} (–SH) [35,36]. The ChiCys sample presents bands associated with stretching and bending vibrations of the C–H and CH_2 species at 2,800–3,000 and 1,492 cm^{-1}, respectively, stronger than in the Chi spectra. As a consequence, the contributions of Cys of the chitosan polymer [36]. Furthermore, the ChiCys sample presents a minor signal at 540 cm^{-1}, which indicated the formation of disulfide bonds (S–S) by adjacent thiol groups [37]. As, the deformation $\varrho(CH_2)$ in phase at 760 cm^{-1}, only appeared at ChiCys, some other less intense bands (not highlighted) at ChiCys were observed: The cis and trans (C–C) stretching at 1,037 and 1,100 cm^{-1}, respectively, the C=O stretching region appears at 1,766 cm^{-1} (not highlighted) and the band at 1,064 cm^{-1} (not highlighted), characteristic of a random (C–C) skeletal conformation [36].

Through the functionalization of chitosan, the protons in the thiol groups can be easily replaced by D from the D_2O used for NMR sample preparation, making them undetectable in the NMR spectrum, the nuclear magnetic resonance spectroscopy has been widely used as a characterization tool for evaluating polysaccharides such as chitosan and its functionalized derivatives [38]. In this sense, ^{1}H-NMR spectroscopy was used as a supporting technique for further investigating the functionalization of the chitosan backbone by thiol modifier. In the H^1 NMR spectra of Chi, it is observed a signal at δ = 2.0 ppm associated with the hydrogen of methyl groups of the acetamide moieties ($NHCOCH_3$) [23,32] (Fig. S3), as at ChiCys sample (Fig. 1d). Additionally, the signal observed at δ = 3.05 ppm corresponds to the hydrogen bonded to the carbon atom C1 of the glucosamine ring. In the region between 3.0 and 3.5 ppm of the ^{1}H NMR spectra of ChiCys, it can be observed that the Cys at the backbone of CHI in the amino groups [26,35]. In addition, in the spectra of ChiCys the representative example displaying a well-defined peak at 1.2 ppm related to alkyl-SH and the proton peak resonate at 2.8 and 3.1 ppm was ascribed to the side-chain methylene (CH_2SH), with the reports from other authors [19,26,38]. These results confirmed that Cys was successfully grafted onto the chitosan backbone forming thiomer-functionalized structures.

3.1.3. Analysis of swelling degree and gel-fraction of 3D scaffolds

The swelling behavior showed that the chitosan (chi reference) had the best adsorption (Fig. 2a). Therefore, the behavior of gel-fraction was the opposite (Fig. 2b). Schmitz et al. [22] studied the stability of thiol chitosan in aqueous solutions at pH 5 and 6. They demonstrated that the thiol groups were subject to an oxidation process leading to a rapid pH dependency formation of disulfide bonds. Other authors [39,40] showed that the reactivity and accessibility of the thiol group will strongly depend on the pH. Moreover, the L-cysteine has two other terminal groups that are chemically active, $–NH_2$ and –COOH, besides the –SH. These groups are depending on the pH, which may play a role in the formation and organization of the monolayer [39,40]. A significant decrease of the swelling degree (SD) at equilibrium of chitosan (4,595 ± 540) for the ChiCys (2,459 ± 251) was observed after 24 h of immersion in deionized water (pH = 5.5 ± 0.5, at room temperature, 26°C ± 2°C). This behavior was expected, as the hydrophobic nature of thiol group incorporated in ChiCys [22,28]. Although several methods are reported in the literature for evaluating the swelling degree of hydrogels, most of them present well-correlated results with no relevant difference for the overall tendency analyzed. These results are consistent with the FTIR findings and the degree of functionalization, where the thiolation of chitosan occurred via the formation of amide bonds (i.e., replacing $–NH_2$ groups by –SH groups), which led to a more chemically hydrophobic polymer matrix for water swelling. Furthermore, that is very common in swelling measurements of 3D scaffolds made by freeze-drying process using highly hydrophilic polymers such as chitosan and derivatives associated with the high surface area and porosity (i.e., >80%). In addition, swelling measurements are dependent on the different methods and conditions (e.g., pH, buffer, temperature, weighing, etc.)

usually reported in the literature [23,28], which may explain the higher standard deviation.

3.1.4. Morphological analysis of 3D scaffolds

The combination of morphological features favors the permeability and flux of adsorbate, supporting the adsorption of azo dyes by the scaffolds. So, it is very important to understand the morphology of scaffold, in particular porosity. This parameter strongly affects the mechanical and adsorption performance of the developed structures. In this sense, SEM micrographs of samples are shown in Fig. 3. The SEM images show a porous structure and a laminar structure present in samples, which are similarly described in the literature, where it was observed that the thiol chitosan exhibited a highly macro-porous sponge-like structure [41]. In addition, the pores present an interconnected structure and the average pore diameters are 223 ± 72 μm. These interconnected pores are very important to facilitate the diffusion of the adsorbate [6,42].

To support the SEM results, the micro-CT showed that scaffolds present highly porous structures with a reasonably monodisperse distribution in the 3D volume. Moreover, these systems also present distinct architectural aspects, such as pore distribution and connectivity. The average wall thickness of the ChiCys scaffold was 83 μm. The results demonstrated average pore sizes of approximately 204 ± 6 μm (Fig. 3). In addition, the porosity was 86% ± 4%. It is noticeable the hydrophobic characteristic of Cysteine, probably influenced the pore hierarchy. The repulsive forces between ChiCys and water, associated with system thermodynamics, reduced the free energy of the hydrophobic ChiCys accelerating the process of freeze-drying. Architectural parameters such as the pore size, interconnectivity and surface area/volume ratio (*S*/*V*) of scaffolds are summarized in Table 1. These results supported the SEM analysis presented before.

To complete the morphological analysis of 3D scaffolds, the surface area was determined by BET. This method indicated that the surface area is 10 $m^2 g^{-1}$. The high porosity of the scaffolds and their high surface area likely provided a very large surface-to-volume ratio, thus offering abundant active sites for the adsorption of azo dyes [43].

3.1.5. Characterization of biological toxicity of 3D scaffold sorbents

The toxicity of scaffolds was characterized using an MTT in vitro assay according to the international standard described at section 2.3.6 as a preliminary assessment of potential applications as environmentally friendly adsorbents for wastewater treatment [33]. HEK 293 T cells were used as a model cell line, as they have been widely applied in basic and applied research owing to their ease of access, highly proliferative behavior, and the repeatability of results in experiments. However, it is not recommended to directly extrapolate the response of HEK 293 T cell cultures in vitro to consider the tested material safe to health and

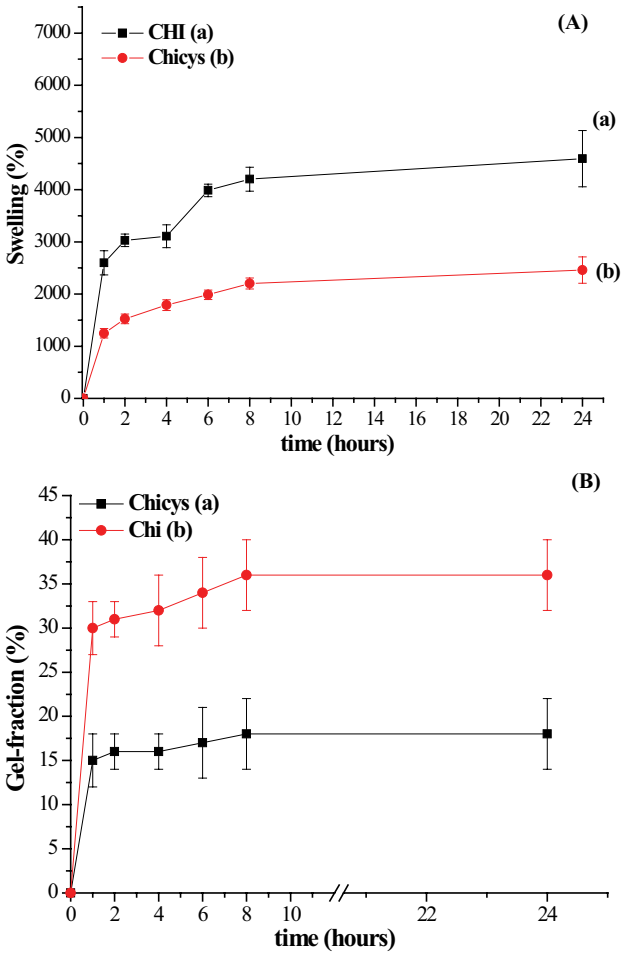

Fig. 2. (A) Swelling degree at deionized water (pH = 5.5 ± 0.5) at function of time and (A) gel fraction at deionized water (pH = 5.5 ± 0.5) at function of time.

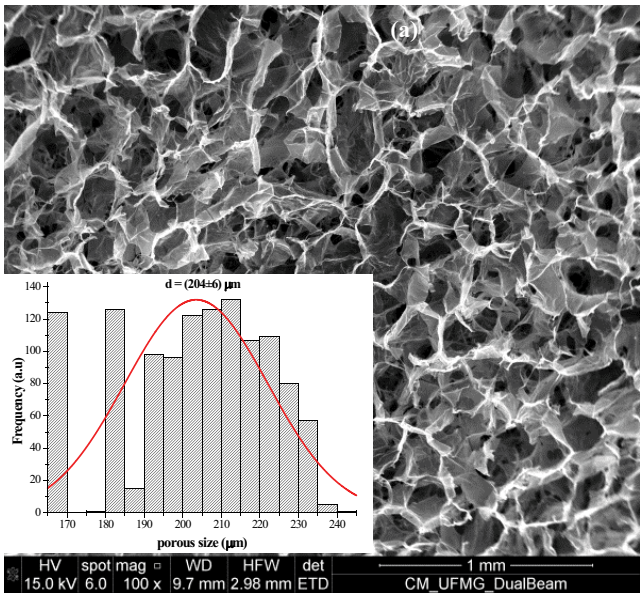

Fig. 3. SEM images at 100× and distribution of porous size of Chicys (inset).

Table 1
Morphological characteristics of porous matrices of ChiCys by micro-CT analysis (software v.1.15.4.0, Bruker micro-CT, Belgium)

Morphological characteristics	ChiCys
Average pore size (μm)	204 ± 6
Porosity (%)	86 ± 4
S/V (μm^{-1})	0.026 ± 0.003
Interconnectivity (%)	>90

the environment [33]. Fig. 4 shows that scaffolds induced no cytotoxic effects, as there were cell viability responses of approximately 90%, similar to the reference control condition (100%, within statistical variation). Despite differences in the physicochemical properties of scaffolds, they demonstrated to be non-toxic towards HEK 293 T cells. This was attributed to the high biocompatibility of naturally derived polymers such as chitosan and its derivatives favoring the cell activity. Moreover, based on the aforementioned results, highly adsorbent scaffolds presented satisfactory physicochemical properties and biocompatibility for their evaluation as innovative systems for the adsorption of azo dyes from aqueous medium.

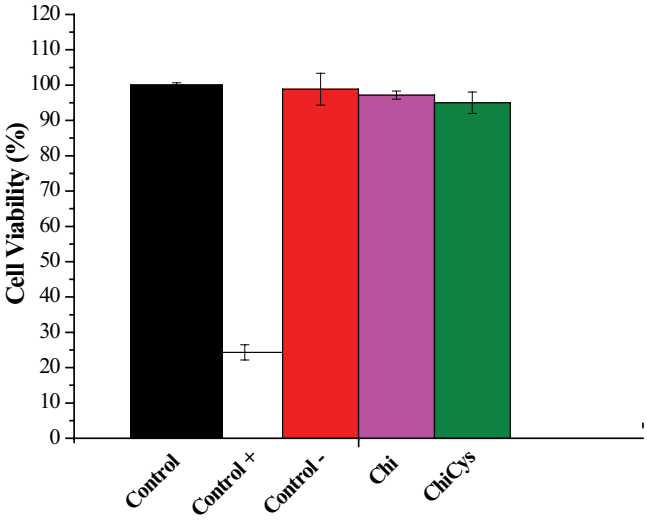

Fig. 4. Histogram of cell viability of embryonic cell lines (HEK) towards all samples.

3.2. Analysis of dye adsorption process

3.2.1. Adsorption analysis of MO

The scaffolds were coiled and immersed in the MO solution at an initial concentration of 20 mg.L^{-1} (pH = 7.0 ± 0.5) for 24 h to verify the adsorption–desorption equilibrium of bio-sorbents and the results are presented in Fig. 5. After the immersion of scaffold adsorbents, the MO adsorption was verified by the significant decrease of the band previously related to the MO dye (Fig. S4). In addition, the adsorption capacity and the adsorption efficiency showed that the scaffold behaved as effective adsorbents of MO 148 ± 5 mg g^{-1} and 91% ± 2% for the concentration of 20 mg L^{-1}.

It seemed that the thiol group significantly influenced the adsorption of MO anionic dye as an organic pollutant by the higher concentration of thiol, resulting in the formation of an MO–thiolate complex on the scaffold surfaces. Strong electrostatic forces probably formed due to a linkage formed between the oxygen present in MO and the thiol on the

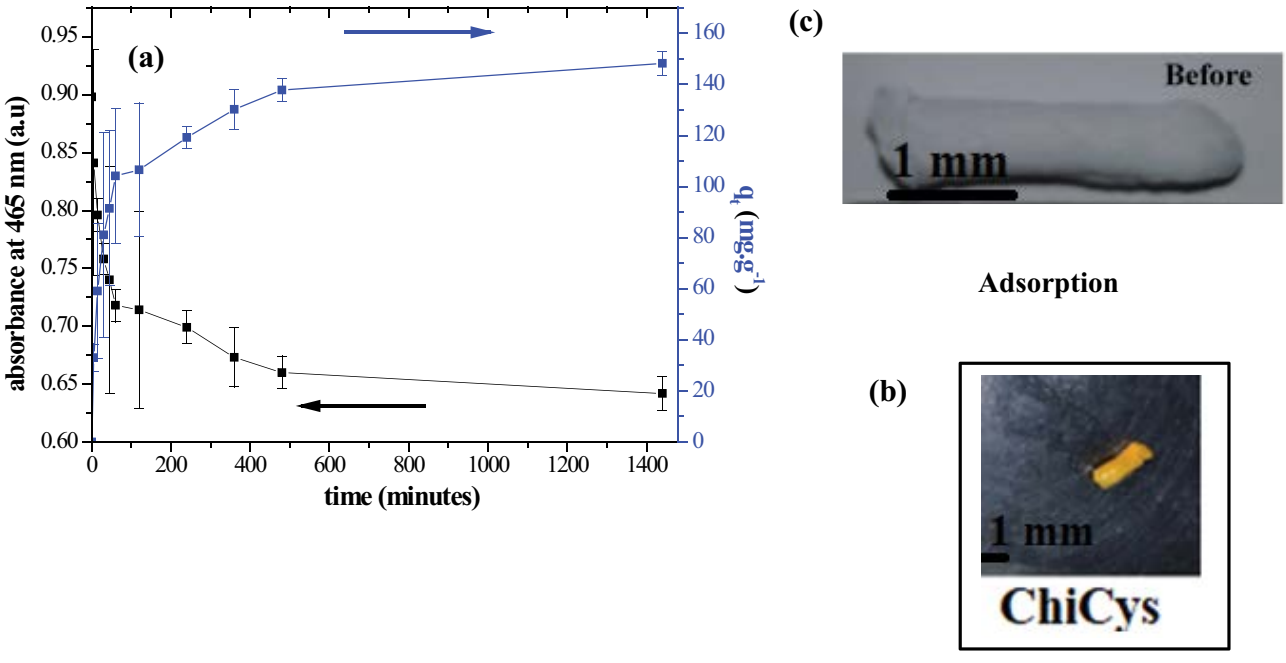

Fig. 5. (a) Adsorption capacity and absorbance modification of MO as a function of time (q_t); (b) Illustration of samples after 24 h in contact with MO; (c) ChiCys before the adsorption process.

ChiCys favoring the adsorption process by the formation of a thiol–MO dye complex. Moreover, these results presented a high adsorption capacity compared with other studies in the literature (Table 2).

Raman spectroscopy was used to investigate the role of thiol groups on MO adsorption. The Raman spectra showed the interaction between MO and the thiol at ChiCys by the decrease of bands at 610 cm^{-1} (–C–S), 540 cm^{-1} (S–S) and 2,560–2,500 cm^{-1} (–SH). Moreover, the ratio of the reference band intensity at 2,885 cm^{-1}, which was not significantly affected by the chemical reaction with MO, and the intensities of the 540 cm^{-1} (S–S) and 2,560–2,500 cm^{-1} (–SH) bands were used to confirm the adsorption mechanism (Fig. 6). The decrease of this ratio indicates the interaction of thiol groups with MO during adsorption. These results help conclude that only a special type of S–S bond is involved in MO adsorption. In fact, the atoms involved in the disulfide bonds (C–C–S–S–C–C) of adsorbent structure can assume different spatial orientations, causing three contrasting conformations for the chemical bonds: trans–gauche–trans, gauche–gauche–trans and gauche–gauche–gauche [47]. The S–S stretching vibration at 540 and 525 cm^{-1} is the trans-gauche–trans and gauche–gauche–trans conformations, respectively, while for the gauche–gauche–gauche it is 510 cm^{-1} [47]. The results indicated that the trans-gauche–trans disulfide bridges prevail in the ChiCys and were preferably consumed during MO adsorption. Moreover, the sharp band at 2,550 cm^{-1} (ν(S–H) vibrational mode) shown in the ChiCys spectrum disappears after reaction with MO, which confirms that the thiol group resulted in the formation of a MO-thiolated chitosan complex on the scaffold surface.

Table 2
Maximum adsorption capacity of various materials modified for adsorption of MO and others ions reported in the literature

Reference	Adsorbent	q_{max} (mg g^{-1})
[6]	Aminated pumkin seed powder Zr (IV)-immobilized crosslinked	4.9
[43]	Chitosan/bentonite composite	76.9
[44]	Chitosan spheres	5.8
[45]	Chitosan biomass	29
[46]	Chitosan/alumina composite	32.999
This study	ChiCys	305 ± 2

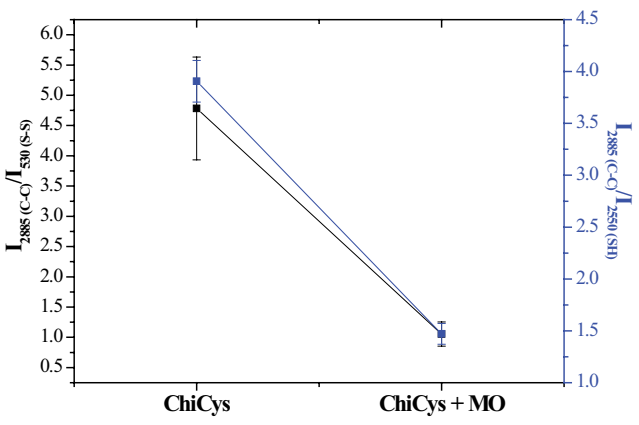

Fig. 6. Relationship between band intensities at 2,885 and 2,550 cm^{-1} and between bands at 2,885 and 530 cm^{-1}.

The pH of the solution will affect both the charges of the ionized MO molecules and the thiol group, thus the adsorption process. This study was conducted at pH 3.0 ± 0.2 to 9.0 ± 0.2 (adjusted with NaOH or HCl 1.0 mol L^{-1}) on the adsorption of MO solutions (20 mg L^{-1}). Before and after scaffold immersion and with increasing time intervals, aliquots of the MO solutions were collected and analyzed to determine the dye concentration. The effect of acid and alkaline conditions on MO or adsorption was also studied and is shown in Fig. 7.

Under basic conditions, over pKa of MO (MO pKa = 4.6 provided by the manufacturer, and confirmed by the zeta potential), MO protonates: the amino group to form an ammonium ion ($R–NH_3^+$) or the azo group to form an azonium ion ($R = NH_2^+$) [45]. As pH decreases, the MO charge changes from positive to neutral and finally to negative

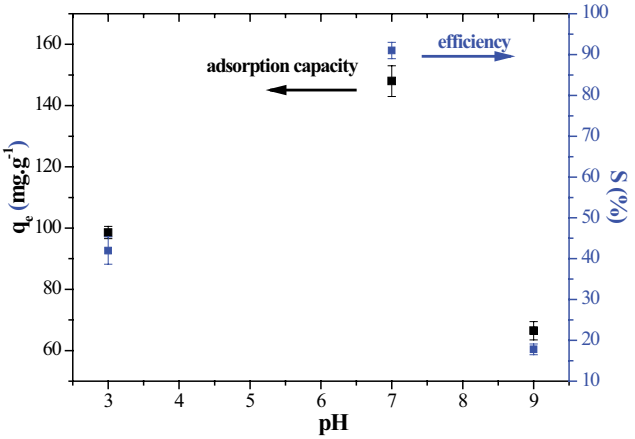

Fig. 7. Uptake of methyl orange (MO) by CHIMerc at different pH. Experimental conditions: MO initial concentration 20 mg L^{-1}; temperature of 26°C ± 2°C.

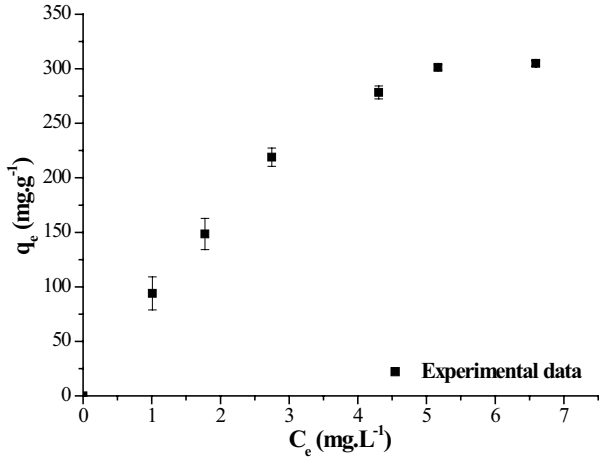

Fig. 8. Isotherm of MO adsorption by ChiCys.

charge [48]. Moreover, under acid conditions, below pKa of MO, the sulfonate group (–SO_3H) in the molecular structure of the MO can be converted in aqueous medium into active negative sulfonate group (–SO_3^-) [48]. The study of the effect of pH was developed at pH (9.0 ± 0.2), (7.0 ± 0.2) and (3.0 ± 0.2). All along the adsorption experiments, pH variation was less than 0.2 units, which indicates that no net release of H^+ or OH^- groups.

The obtained results showed the highest MO uptake at neutral conditions, thus indicating that the charge of MO does not influence directly methyl orange adsorption on ChiCys. Adsorption is rather dominated by the great affinity of MO by the thiol groups (Fig. 7). At neutral conditions, the polymer chain increases the formation of dative bonds (electron donor: :NH_2 or :SH), and the kinetics of thiol oxidation is very slow, as demonstrated in previous section by Raman spectroscopy. Under acid conditions, the amine groups of ChiCys are predominantly protonated (NH_3^+) and the sulfonate group (–SO_3H) in the molecular structure of the MO can be converted in aqueous medium into active negative sulfonate group (–SO_3^-), which provides a strong electrostatic (columbic) attraction between positively charged of the amine groups of ChiCys are predominantly protonated (NH_3^+) [48]. Under basic conditions, the oxidation process of a thiol group takes place, as demonstrated by the Raman analysis, the amino group does not protonate, and the MO protonates into ammonium ion (R–NH_3^+) or the azo group to form an azonium ion (R = NH_2^+) [48], which may contribute to decreased MO adsorption.

The Langmuir and Freundlich equations [49] were tested to determine the best model to describe the results, in a concentration range of 0–100 mg L^{-1}, mass of adsorbent of 13 mg, final pH of 6.5 ± 0.5 and temperature of 26°C ± 2°C. The Langmuir equation is given as follows:

$$q_e = \frac{\left(K_L C_e q_m\right)}{\left(1 + K_L C_e\right)} \tag{2}$$

The Langmuir constant (K_L) is used to calculate R_L, a dimensionless separation factor given by Eq. (3) [49] as follows:

$$R_L = \frac{1}{\left(1 + K_L C_0\right)} \tag{3}$$

The R_L values indicate whether the adsorption is unfavorable ($R_L > 1$), linear ($R_L = 1$), favorable ($0 < R_L < 1$), or irreversible ($R_L = 0$) [49].

The Freundlich isotherm is an empirical equation and is one of the most widely used isotherms for the description of multi-site adsorption. Mathematically, it is expressed by Eq. (4) [49], where K_F (mg L^{-1}) is a constant relating the adsorption capacity and $1/n$ is an empirical parameter relating the adsorption intensity.

$$q_e = K_F C_e^{1/n} \tag{4}$$

The amount of solute adsorbed per unit mass of the adsorbent in equilibrium with the concentration of an adsorbate in bulk solution at a given temperature may be expressed by an adsorption isotherm. The two most common equations for describing solid–liquid sorption systems are the Langmuir and Freundlich (two-parameter isotherms) [6,49]. The constants K_L, K_F, R_L, and q_m are presented in Table 4.

The best fitting was achieved with the Langmuir equation, as shown by R^2 and the average absolute percentage deviation (%D) (Eq. (5)) [11] (Table 3). The adsorption involves the affinity of thiol groups, crafted on the chitosan chain, by the oxygen in the MO pigment. It is also noticeable that the development of a plateau corresponding to a maximum adsorption capacity of 305 ± 2 mg g^{-1}, (Fig. 8) which is relatively high if compared with the other studies reported in the literature (Table 4) in similar systems.

$$D\% = \left(\frac{1}{N} \sum_{i=1}^{N} \sum \left| \frac{\left(q_{e,\exp} - q_{e,\mathrm{cal}}\right)}{\left(q_{e,\exp}\right)} \right| \right) \times 100 \tag{5}$$

where N is the number of experimental points; and $q_{e,\exp}$ and $q_{e,\mathrm{cal}}$ are the experimental data and calculated amounts adsorbed, respectively.

Table 3
Parameters of Langmuir's and Freundlich's equations

Methyl Orange								
Langmuir					Freundlich			
q_m (mg g^{-1})	K_L (L mg^{-1})	R_L	R^2	D(%)	K_F (mg g^{-1})	n	R^2	D(%)
305.24	0.75	0.063	0.9952	5	3.21	2	0.98974	12
Methylene Blue								
Langmuir					Freundlich			
q_m (mg g^{-1})	K_L (L mg^{-1})	R_L	R^2	D(%)	K_F (mg g^{-1})	n	R^2	D(%)
115	0.42	0.05	0.9991	4	2.1	1	0.9755	15

q_m (maximum uptake obtained by the Langmuir equation); K_L (Langmuir constant); R_L (dimensionless separation factor); K_F (constant relating the adsorption capacity); n (empirical parameter related to the deviation of linearity); D (average absolute percentage deviation).

Table 4
Comparison of various materials modified for adsorption of dyes reported in the literature

Reference	Adsorbent	q_{max} (mg g^{-1})	%*S*	Desorption (%)	Adsorbate
[6]	Aminated pumkin seed powder Zr (IV)-immobilized crosslinked	126.1	79	65	MO
[42]	Porous carbon monolith	80	80	40	MB
[42]	Nanocrystalline cellulose	90		90	MB
[44]	Chitosan spheres	5.8	–	–	MO
[45]	Chitosan biomass	29	–	–	MO
[46]	Chitosan–alumina composite	32.999	92,84	84.91	MO
[50]	Chitosan-coated cotton	–	90	–	Congo Red
[51]	Chitosan magnetic composite	100	96	~60	MO
[52]	HEMA-chitosan-MWCNT nanocomposite	198	–	–	MO
This study	ChiCys	115 ± 2	30 ± 2	32 ± 1	MB
This study	ChiCys	305 ± 2	91 ± 2	52 ± 1	MO

3.2.2. Kinetic analysis of MO adsorption

The adsorption kinetics of the dye was calculated by monitoring the absorbance of the MO solution. In Fig. 5 it was clearly noticeable that the adsorption capacity of the dye increased rapidly in the initial stages and slowed down as equilibrium was attained at approximately 240 min. According to the literature, two types of kinetics are generally used for the study of adsorption processes, namely, the pseudo-first-order and pseudo-second-order rate laws [6,11]. For the scaffolds, the pseudo-second-order model fitted better the adsorption data as attested by the higher correlation coefficient (R^2), compared with the first-order kinetics (Fig. 9b; Table S1). Therefore, the Chi square (χ^2) test, a non-parametric test that can be used to determine the best fitted model, was used to confirm the results ($R^2 = 0.998$, $\chi^2 = 0.4265 << \chi^2_c = 18.924$ with significance level of 0.05; degree of freedom = 9 for ChiCys).

The theoretical value of q_e was 148 mg g^{-1} for the concentration of 20 mg L^{-1}. The pseudo-second-order rate constant calculated from Fig. 9 was 4×10^{-3} g mg^{-1} min^{-1}, and both data agree very well with the experimental data. These results suggest that the adsorption of MO by thiolated chitosan fitted properly with the pseudo-second-order kinetic model, which relies on the assumption that the process is controlled by the adsorption reaction at the liquid/solid interface of the adsorbent [11,33].

The pseudo-second-order reaction kinetics model provided the best correlation with the experimental data, indicating that adsorption of MO by the scaffolds was governed

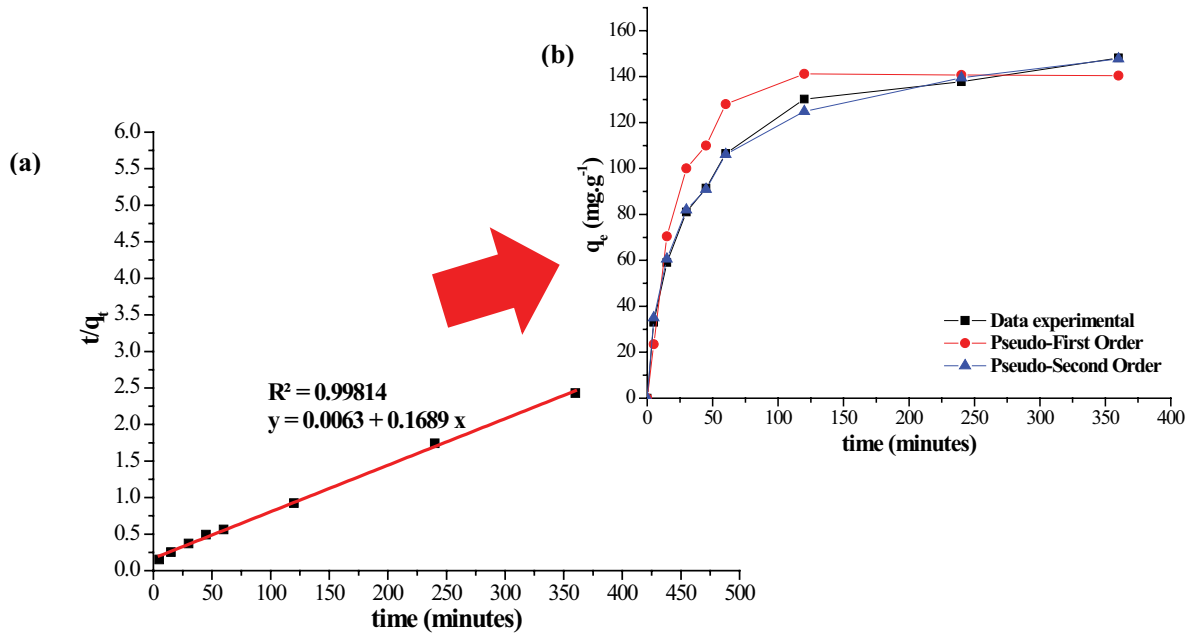

Fig. 9. (a) Kinetics at 480 min of ChiCys pseudo-second-order; (b) comparison of amount adsorbed among experimental data (black line), pseudo-first-order (red line) and pseudo-second-order (blue line) of ChiCys.

by the chemisorption process. However, during a solid/liquid adsorption process, adsorbate transfer may be driven by liquid/phase mass transport (boundary layer diffusion) or intraparticle mass diffusion or both. These phenomena are very complex and subject to several aspects and properties of the adsorbent–adsorbent systems that are beyond the scope of this study. Nonetheless, as an exploratory assessment of this subject, the intraparticle diffusion model (IDM) was tested and it is showed in Fig. S5.

3.2.3. Analysis of MB dye adsorption

The immersion of the scaffolds in the aqueous solution with MB dye resulted in less adsorption than MO as shown in Fig. 10a. The scaffolds presented an MB adsorption capacity of 57 ± 6 mg g^{-1} for the concentration of 20 mg L^{-1}. These results demonstrated that the thiol group has an important role for the mechanism of dye adsorption and the amount of this group attracted the specific dye, and the adsorption is rather dominated by the great affinity of MO by the thiol groups. Nonetheless, the surface area and porosity probably provided sites for physio-sorption which overcame the attraction from the thiol group of the dye.

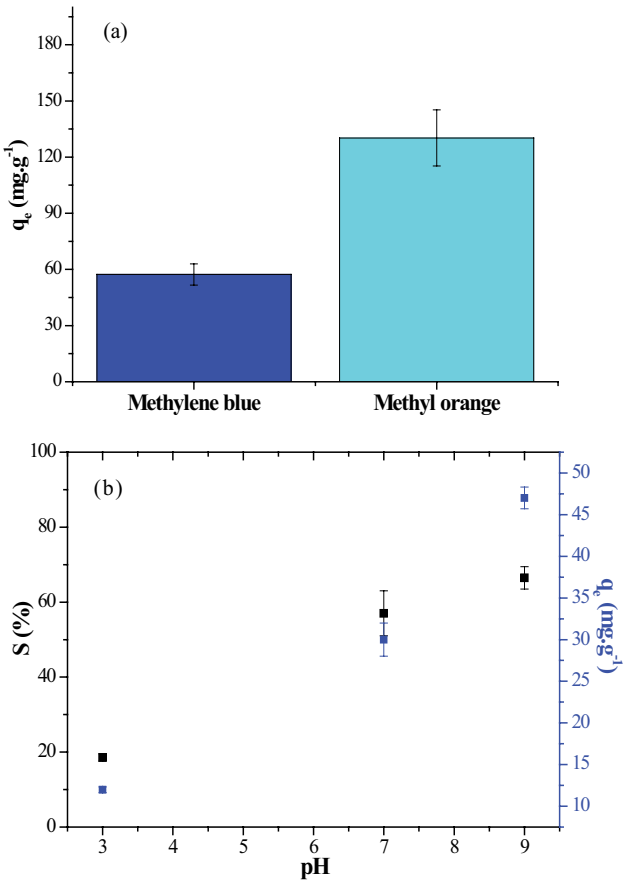

Fig. 10. (a) Comparison between adsorption efficiency of methylene blue and methyl orange of ChiCys at 20 mg L^{-1} and (b) uptake of methyl orange (MB) by ChiCys at different pH. Experimental conditions: MB initial concentration 20 mg L^{-1}; temperature of 26°C ± 2°C.

The pH of the solution will affect both the charges of the ionized MB molecules and the thiol group. In this sense, this study tested the effect of pH on the MB adsorption by ChiCys. The analysis was conducted at pH 3.0 ± 0.5 to 9.0 ± 0.5 (adjusted with NaOH or HCl 1.0 mol L^{-1}) on the adsorption of MB solutions (20 mg L^{-1}). Before and after scaffold immersion and with increasing time intervals, aliquots of the MB solutions were collected and analyzed to determine the dye concentration. The effect of acid and alkaline conditions on MB or adsorption was also studied and is shown in Fig. 10b.

In the case of MB, it was observed a great relevant effect on the adsorption capacity using MB solutions under basic (pH = 9.0 ± 0.2) conditions compared with MO adsorption. At neutral conditions, the polymer chain increases the formation of dative bonds (electron donor: :NH_2 or :SH), and the kinetics of thiol oxidation is very slow, as demonstrated in previous section by Raman spectroscopy. Therefore, the MB adsorption in this pH was smaller than MO adsorption. Under acid conditions, the amine groups of ChiCys are predominantly protonated (–NH_3^+) and MB is positively charged (MB^+), so a repulsive force prevails. Nevertheless, under basic conditions, the MB adsorption was greater than others (Table 4). Probably, because the presence of electron donor by :NH_2, or :SH added the presence of free electrons from the hydroxyl group (:OH) present at ChiCys, which may be a great role in the MB adsorption. However, in any pH, the MB adsorption was smaller than MO, which confirms that the thiol group resulted in the formation of a MO-thiolated chitosan complex on the scaffold surface and showed a great affinity by this specific dye.

Similar to MO, it was conducted the isotherms for MB. The best fitting was achieved with the Langmuir equation, as shown by R^2 and the average absolute percentage deviation (%*D*) (Eq. (5)) [11] (Table 3). It is also noticeable the development of a plateau corresponding to a maximum adsorption capacity of 115 ± 2 mg g^{-1} (Fig. 11), which is relatively high if compared with the other studies reported in the literature (Table 4) in similar systems.

3.2.4. Analysis of MO and MB desorption

To offer the possibility of recuperating the MO and MB extracted from the adsorbent and liquid phase, it is desirable to reestablish the adsorbent material. For this experiment, four systems (EDTA, KCl, HNO_3, and NaOH) were chosen. The recovery of MO after the first cycle was 52% ± 1%, 46% ± 2% and 27% ± 2% for the EDTA, KCl and HNO_3, respectively, and for each cycle is shown in Fig. 12a. In this figure, it can be observed that there was a decrease of 26% approximately, when comparing the first with the third cycle when the HNO_3 was used, but in the case of EDTA or KCl onward the amount adsorbed remained practically constant, the decrease was very little, approximately 8%. In the case of MB, the recovery was a much smaller when compared with MO. The recovery of MB after the first cycle was 32% ± 1%, 26% ± 2% and 13% ± 2% for the EDTA, KCl and HNO_3, respectively, and for each cycle is shown in Fig. 12b. Therefore, the behavior of each solution used in desorption process was the same. These results indicated the potential use of these new 3D scaffolds as eco-friendly bio-sorbents

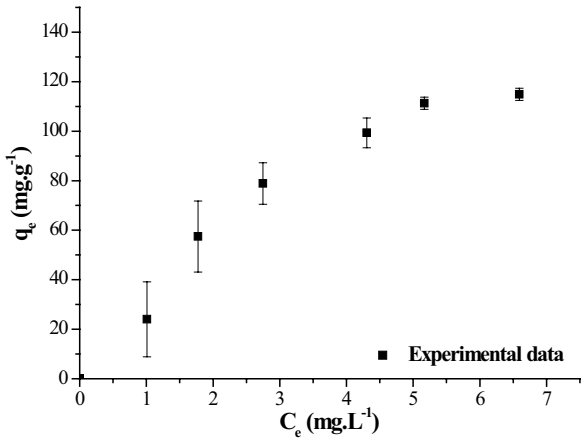

Fig. 11. Isotherm of MB adsorption by ChiCys.

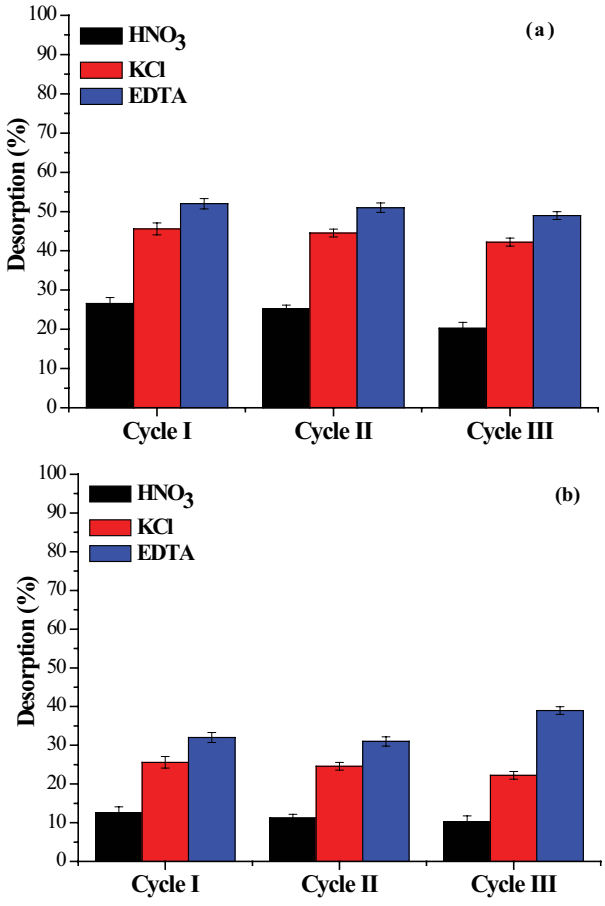

Fig. 12. (a) Desorption of methyl orange from ChiCys by different media T = 26°C ± 2°C for each cycle and (b) desorption of methylene blue from ChiCys by different media T = 26°C ± 2°C for each cycle.

and biocompatible for MO and MB removal and recovery in environmental applications. Furthermore, the results also demonstrate the chemical stability of adsorbents. The excellent reusability of the sorbents will save cost for MO or MB removal thus have huge economic benefits.

3.2.5. Comparison with the literature

A comparison with other green adsorbents is also provided and it shows that the adsorbent of this study presented a great MO adsorption (Table 4). The results showed a smaller MO and MB adsorption compared with the adsorbent in this study. These results confirm that the chitosan thiolated remains competitive compared with others conventional adsorbents. Moreover, this adsorbent showed a non-toxic property, which confirm the use of eco-friendly bio-sorbents and biocompatible for MO and MB removal and recovery in environmental applications.

4. Conclusions

This study presented the synthesis and comprehensive characterization of novel soft eco-friendly and biocompatible 3D scaffolds based on thiolated chitosan using a green aqueous process, as a model for the dye adsorption. The results demonstrated that the morphological and physicochemical features were modified by the extent of thiol modification. These thiomer derivatives were subsequently grafted with cysteine to create thiol-modified chitosan and the thiolation was higher than other reports in literature. The average pore size and porosity provided a very large surface-to-volume ratio, which offer abundant active sites for the adsorption. These scaffolds presented no toxicity based on approximately 90% of the live cell viability responses using an MTT assay. Moreover, there are no works observed in the literature about the relationship between thiolated chitosans and pigments. These 3D thiomers behaved as effective bio-sorbents for the adsorption of MO used as a model of dye pollutant in water. The typical adsorption efficiency of over 90% was attributed to the formation of thiolated chitosan–dye complexes. The pseudo-second-order kinetic model was well fitted describing the adsorption of MO, which shows that the maximum adsorption capacity is highly dependent on the chemical structures of the dye and absorbents. The maximum adsorption capacity was about 305 and 115 mg g^{-1} for MO and MB, respectively, which is higher than similar studies with other chitosan derivatives. Finally, the scaffolds showed that the MO and MB recovery was over 50% and 32%, respectively, which will save cost for MO removal thus have enormous economic. Thus, these 3D scaffolds are envisioned as promising low-cost bio-sorbents for potential wastewater treatment.

Acknowledgments

The author acknowledges the financial support from the Universidade Federal dos Vales do Jequitinhonha e Mucuri (UFVJM), and expresses her gratitude to the Chemistry and Odontology Department of UFVJM for the SEM/EDX, BET, micro-CT, and the spectroscopy analyses.

References

[1] I. Ali, K. Gupta, Advances in Water Treatment by Adsorption, Taylor & Francis, New York, 2007.
[2] Z. Aksu, Application of biosorption for the removal of organic pollutants: a review, Process. Biochem., 40 (2005) 997–1026.
[3] N. Peng, D. Hu, J. Zeng, Y. Li, L. Liang, C. Chang, Superabsorbent cellulose-clay nanocomposite hydrogels for highly efficient removal of dye in water, ACS Sustain. Chem. Eng., 4 (2016) 7217–7224.

[4] F. Alakhras. Biosorption of Cd(II) Ions from aqueous solution using chitosan-iso-vanillin as a low-cost sorbent: equilibrium, kinetics, and thermodynamic studies, Arab. J. Sci. Eng., 44 (2018) 279–288.
[5] B. Halling-Sorensen, S.N. Nielsen, P.F. Lanzky, F. Ingerslev, H.C.H. Lützheft, S.E. Jorgensen, Occurrence, fate and effects of pharmaceutical substances in the environment – a review, Chemosphere, 36 (1998) 357–393.
[6] M.V. Subbaiah, D-S Kim. Adsorption of methyl orange from aqueous solution by aminated pumpkin seed powder: kinetics, isotherms, and thermodynamic studies, Ecotoxicol. Environ. Saf., 128 (2016) 109–117.
[7] X. Li, Y. Li, S. Zhang, Z. Ye. Preparation and characterization of new foam adsorbents of poly(vinyl alcohol)/chitosan composites and their removal for dye and heavy metal from aqueous solution, Chem. Eng. J., 183 (2012) 88–97.
[8] E. Emmanuel, Y. Perrodin, G. Keck, J.M. Blanchard, P. Vermande, Ecotoxicological risk assessment of hospital wastewater: a proposed framework for raw effluents discharging into urban sewer network, J. Hazard. Mater., A, 117 (2005) 1–11.
[9] A. Bhatnagar, M. Sillanpää, A. Witek-Krowiak, Agricultural waste peels as versatile biomass for water purification — a review, Chem. Eng. J., 270 (2015) 244–271.
[10] M.S.D. Erosa, T.I.S. Medina, R.N. Mendoza, M.A. Rodriguez, E. Guibal, Cadmium sorption on chitosan sorbents: kinetics and equilibrium studies, Hydrometallurgy, 61 (2001) 157–167.
[11] R. Laus, V.T. Fávere, Competitive adsorption of Cu (II) and Cd (II) ions by chitosan crosslinked with epichlorohydrin-triphosphate, Bioresour. Technol., 102 (2011) 8769–8776.
[12] M. Monier, Adsorption of Hg^{2+}, Cu^{2+} and Zn^{2+} ions from aqueous solution using formaldehyde cross-linked modified chitosan-thioglyceraldehyde Schiff's base, Int. J. Biol. Macromol., 50 (2012) 773–781.
[13] R.K. Gautam, A. Mudhoo, G. Lofrano, M.C. Chattopadhyaya, Biomass-derived biosorbents for metal ions sequestration: adsorbent modification and activation methods and adsorbent regeneration, J. Environ. Chem. Eng., 2 (2014) 239–259.
[14] D.O. Coonery, In: Adsorption Design for Wastewater Treatment, Lewis Publishers, USA, 1999, p. 182.
[15] K.M. Raju, M.P. Raju, Y.M. Mohan, Synthesis of superabsorbent copolymers as water manageable materials, Polym. Int., 110 (2008) 2453–2460.
[16] T. Kamal, M. Ul-Islam, S.B. Khan, A.M. Asiri, Adsorption and photocatalyst assisted dye removal and bactericidal performance of ZnO/chitosan coating layer, Int. J. Biol. Macromol., 81 (2015) 584–590.
[17] S.B. Khan, K.A. Alamry, E. Bifari, A.M. Asiri, M. Yasir, L. Gzara, R.Z. Ahmad, Assessment of antibacterial cellulose nanocomposites for water permeability and salt rejection, J. Ind. Eng. Chem., 24 (2015) 266–275.
[18] S. Gul, Z.A. Rehan, S.A. Khan, K. Akhtar, M.A. Khan, M.I. Khan, M.I. Rashid, A.M. Asiri, S.B. Khan, Antibacterial PES-CA-Ag_2O nanocomposite supported Cu nanoparticles membrane toward ultrafiltration, BSA rejection and reduction of nitrophenol, J. Mol. Liq., 230 (2017) 616–624.
[19] D. Liu, J. Li, H. Pan, F. He, Z. Liu, Q. Wu, C. Bai, S. Yu, X. Yang, Potential advantages of a novel chitosan-N-acetylcysteine surface modified nanostructured lipid carrier on the performance of ophthalmic delivery of curcumin, Sci. Rep., 28796 (2015) 1–14.
[20] M. Croce, S. Conti, C. Maake, G.R. Patzke, Synthesis and screening of N-acyl thiolated chitosans for antibacterial applications, Carbohydr. Polym., 151 (2016) 1184–1192.
[21] F. Talaei, E. Azizi, R. Dinarvand, F. Atyabi, Thiolated chitosan nanoparticles as a delivery system for antisense therapy, Int. J Nanomed., 6 (2011) 1963–1975.
[22] T. Schmitz, V. Grabovac, T.F. Palmberger, M.H. Hoffer, A. Bernkop-Schnurch, Synthesis and characterization of a chitosan-N-acetyl cysteine conjugate, Int. J. Pharm., 347 (2008) 79–85.
[23] W. Mozalewska, R. Czechowska-Biskupa, A.K. Olejnika, R.A. Wacha, P. Ulańskia, J.M. Rosiak, Chitosan-containing hydrogel wound dressings prepared by radiation technique, Radiat. Phys. Chem., 134 (2017) 1–7.
[24] F. Ali, S.B. Khan, T. Kamal, K.A. Alamary, A.M. Asiri, T.R.A. Sobahi, Chitosan coated cotton cloth supported zero-valent nanoparticles: simple but economically viable, efficient and easily retrievable catalysts, Sci. Rep., 7 (2017) 16957.
[25] F. Alakhras, H. Al-Shahrani, E. Al-Abbad, F. Al-Rimawi, N. Ouerfelli, Removal of Pb(II) metal ions from aqueous solutions using chitosan-vanillin derivatives of chelating polymers, Pol. J. Environ. Stud., 28 (2019) 1523–1534.
[26] J.-P. Simonin, On the comparison of pseudo-first and pseudo-second order rate laws in the modeling of adsorption kinetics, Chem. Eng. J., 300 (2016) 254–263.
[27] F. Ali, S.B. Khan, T. Kamal, K.A. Alamary, M. Bakhsh, A.M. Asiria, T.R.A. Sobahi, Synthesis and characterization of metal nanoparticles templated chitosan-SiO_2 catalyst for the reduction of nitrophenols and dyes, Carbohydr. Polym., 192 (2018) 217–230.
[28] D.-Y. Teng, Z.-M. Wu, X.-G. Zhang, Y.-X. Wang, C. Zheng, Z. Wang, C.-X. Li, Synthesis and characterization of in situ cross-linked hydrogel based on self-assembly of thiol-modified chitosan with PEG diacrylate using Michael type addition, Polymer, 31 (2010) 639–646.
[29] R.A.A. Muzzarelli, F. Tanfani, N-(o-carboxybenzyl) chitosan, N-carboxymethyl chitosan, and chitosan dithiocarbamate: new chelating derivatives of chitosan, Pure. Appl. Chem., 54 (1982) 2141–2150.
[30] A. Pestov, O. Koryakova, I. Leonidov, Y. Yatluk, Gel-synthesis, structure, and properties of sulfur-containing chitosan derivatives, Russ. J. Appl. Chem., 83 (2010) 787–794.
[31] S. Chen, G. Wu, H. Zeng, Preparation of high antimicrobial activity thiourea chitosan-Ag^+ complex, Carbohydr. Polym., 60 (2005) 33–38.
[32] K. Kafedjiiski, K.H. Krauland, M.H. Hoffer, A. Bernkop-Schnurch, Synthesis and in vitro evaluation of a novel thiolated chitosan, Biomaterial, 26 (2005) 819–826.
[33] R. Yang, Y. Su, K.B. Aubrecht, X. Wang, H. Ma, R.B. Grubbs, B.S. Hsiao, B. Chu, Thiol-functionalized chitin nanofibers for As (III) adsorption, Polymer, 60 (2015) 9–17.
[34] N. Vallapa, O. Wiarachai, N. Thongchul, J. Pan, V. Tangpasuthadol, S. Kiatkamjornwong, Enhancing antibacterial activity of chitosan surface by heterogeneous quaternization, Carbohydr. Polym., 83 (2011) 868–875.
[35] F.R. de Abreu, S.P. Campana-Filho, Characteristics and properties of carboxymethylchitosan, Carbohyd. Polym., 75 (2009) 214–221.
[36] K. Moller, J. Kobler, T. Bein, Colloidal suspensions of mercapto-functionalized nanosized mesoporous silica, J. Mater. Chem., 17 (2007) 624–631.
[37] M.C. Teixeira, V.S.T. Ciminelli, M.S.S. Dantas, S.F. Diniz, H.A. Duarte, Raman spectroscopy and DFT calculations of As(III) complexation with a cysteine-rich biomaterial, J. Colloid Interface Sci., 315 (2007) 128–134.
[38] X. Liu, B. Yu, Q. Huang, R. Liu, Q. Feng, Q. Cai, S. Mi, In vitro BMP-2 peptide release from thiolated chitosan based hydrogel, Int. J. Biol. Macromol., 93 (2016) 314–321.
[39] M.A.M. Hoffman, P.J.J. van MIL, Heat-induced aggregation of â-lactoglobulin: role of the free thiol group and disulfide bonds, J. Agric. Food Chem., 45 (1997) 2942–2948.
[40] N. Tawill, A. Hatef, E. Sacher, M. Maisonneuve, T. Gervais, R. Mandeville, M. Meunier, Surface plasmon resonance determination of the binding mechanisms of L-cysteine and mercaptoundecanoic acid on gold, J. Phys. Chem., 117 (2013) 6712–6718.
[41] I.-H. Bae, B.-C. Jeong, M.-S. Kook, S.-H. Kim, J.-T. Koh, Evaluation of a thiolated chitosan scaffold for local delivery of BMP-2 for osteogenic differentiation and ectopic bone formation, BioMed. Res. Int., 2013 (2013) 1–11.
[42] X. He, K.B. Male, P.N. Nesterenko, D. Brabazon, B. Paull, J.H.T. Luong, Adsorption and desorption of methylene blue on porous carbon monolits and nanocrystalline cellulose, ACS Appl. Mater. Interface, 5 (2013) 8796–8804.

[43] L. Zhang, P. Hu, J. Wang, Q. Liu, R. Huang, Adsorption of methyl orange (MO) by Zr (IV)-immobilized cross-linked chitosan/bentonite composite, Int. J. Biol. Macromol., 81 (2015) 818–827.
[44] W.A. Morais, A.L.P. Almeida, M.R. Pereira, J.L.C. Fonseca, Equilibrium and kinetics analysis of methyl orange sorption on chitosan spheres, Carbohydr. Res., 343 (2008) 2489–2493.
[45] F.-N. Allouche, N. Yassaa, H. Lounici, Sorption of methyl orange from aqueous solution on chitosan biomass, Proc. Earth Planet. Sci., 15 (2015) 596–601.
[46] J. Zhang, Q. Zhou, L. Ou, Kinetic, isotherm, and thermodynamic studies of the adsorption of methyl orange from aqueous solution by chitosan/alumina composite, J. Chem. Eng. Data, 57 (2012) 412–419.
[47] R.J. Gillespie, E.A. Robinson, The Raman spectra of liquid sulfur trioxide and solutions of sulfur trioxide in inert solvents, Can. J. Chem., 39 (1961) 2189–2200.
[48] A.H. Jawad, N.F.H. Mamat, B.H. Hameed, H. Ismail, Biofilm of cross-linked chitosan-ethylene glycol diglycidyl ether for removal of Reactive Red 120 and Methyl Orange: adsorption and mechanism studies, J. Environ. Chem. Eng., 7 (2019) 102965.
[49] D.G. Kinniburgh, General purpose adsorption isotherms, Environ. Sci. Technol., 20 (1986) 895–904.
[50] N. Ali, Awais, T. Kamal, M. Ul-Islam, A. Khan, S.J. Shah, S. Zada, Chitosan-coated cotton cloth supported copper nanoparticles for toxic dye reduction, Int. J. Biol. Macromol., 111 (2018) 832–838.
[51] D. Yang, L. Qiu, Y. Yang, Efficient adsorption of methyl orange using a modified chitosan magnetic composite adsorbent, J. Chem. Eng. Data, 61 (2016) 3933–3940.
[52] H. Mahmoodian, O. Moradi, B. Shariatzadeha, T.A. Salehf, I. Tyagi, A. Maity, M. Asif, V.K. Gupta, Enhanced removal of methyl orange from aqueous solutions by poly HEMA–chitosan-MWCNT nano-composite, J. Mol. Liq., 2012 (2015) 189–198.

Supplementary information

S1. Kinetics model – equations

S1.1. Pseudo-first-order

$$\ln\left(q_e - q_t\right) = \ln(q_e) - K_1 t \tag{S1}$$

S1.2. Pseudo-second-order

$$\frac{t}{q_t} = \frac{1}{\left(\left(K_2 \times q_e^2\right)\right)} + \left(\frac{1}{q_e}\right) \times t \tag{S2}$$

S1.3. Intraparticle diffusion

$$q\left(t\right) = K_{IP} t^{0.5} + C \tag{S3}$$

where q_e is the amount of dye adsorption per unit of mass of the adsorbent (adsorption capacity at equilibrium, mg g^{-1}); q_t is the amount of dye adsorption per unit of mass of the adsorbent at any given time (t); K_1 is the pseudo-first-order rate constant and it is calculated from the linearization of $\ln(q_e - q_t)$ vs. t at the concentration established at 24 h; K_2 is the pseudo-second-order rate constant (g mg^{-1} min^{-1}) and K_{IP} is the intraparticle diffusion rate constant and the value of C is the boundary layer effect, which gives an idea of the thickness of the boundary layer [22].

Nonetheless, as an exploratory assessment of this subject, the IDM was tested with the mathematical formulation

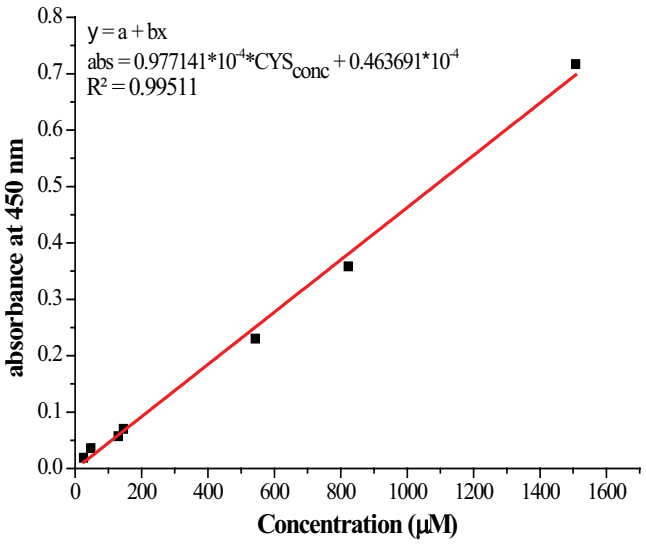

Fig. S1. Calibration curves of cysteine (Cys).

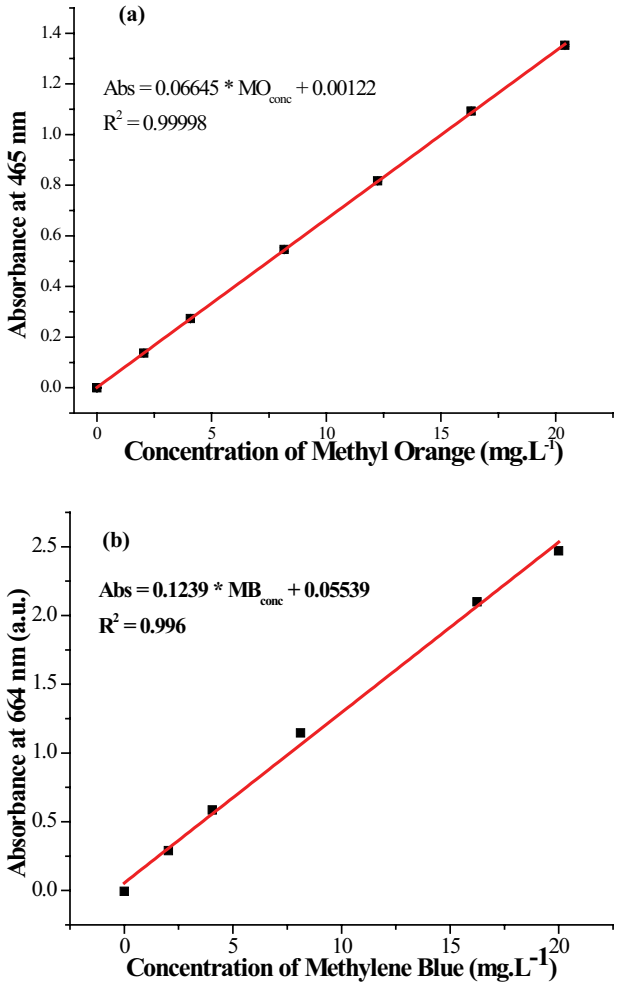

Fig. S2. (a) Calibration curve of Methyl Orange (MO) and (b) calibration curve of Methylene Blue (MB).

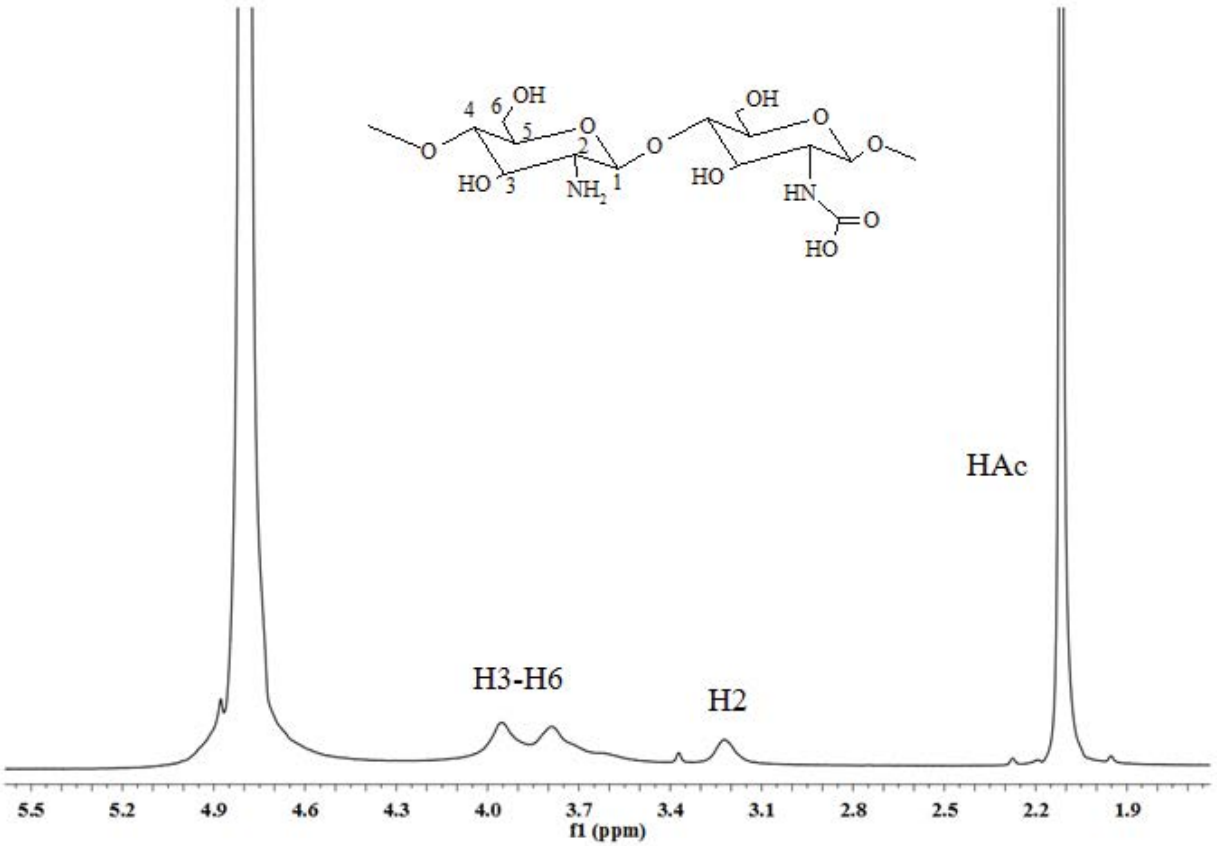

Fig. S3. H^1 NMR spectra of CHI.

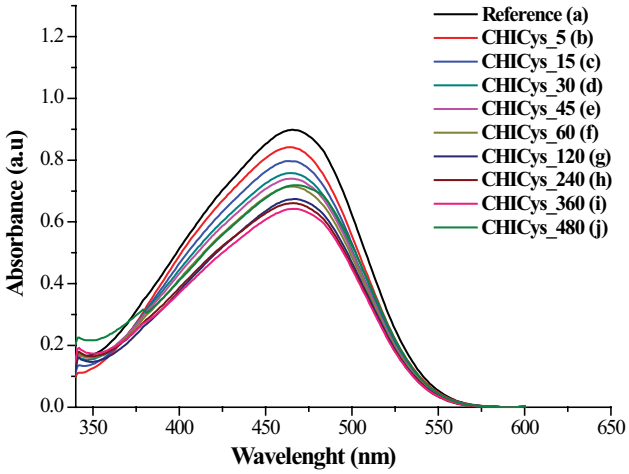

Fig. S4. Change in absorbance of sample Chicys as a function of time of contact with MO with the smallest concentration ((a) Reference, (b) Chicys_5, (c) Chicys_15, (d) Chicys_30, (e) Chicys_45, (f) Chicys_60, (g) Chicys_120, (h) Chicys_240, (i) Chicys_360 and (j) Chicys_480).

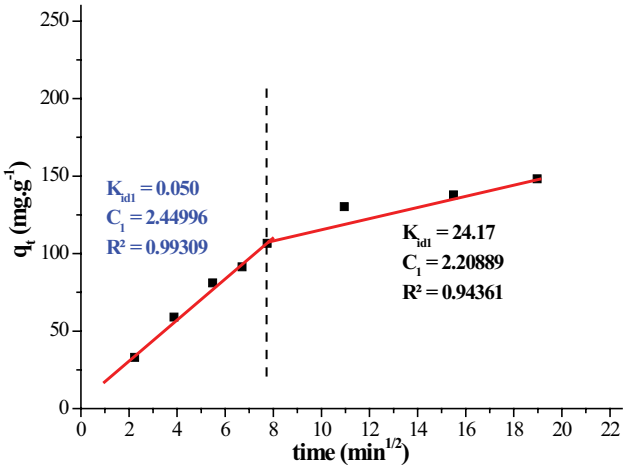

Fig. S5. Kinetics at 480 min of samples (a) Chicys intraparticle diffusion model, (b) CHIMerc intraparticle diffusion model.

Table S1
Pseudo-first-order and pseudo-second-order kinetic parameters for samples Chicys

Sample	Pollutant	Pseudo-first-order		Pseudo-second-order	
		K_1 (min^{-1})	R^2	K_2 (g mg^{-1} min^{-1})	R^2
Chicys	Methyl orange	4.70	0.9431	0.004	0.9981

expressed by Eq. (S3). Fig. S5 presents the IDM plot for the adsorption of MO (20 mg L^{-1}) by the scaffolds, where the parameters $q(t)$ vs. $t^{1/2}$ were fitted by linear correlation (R^2 = 0.85 and R^2 = 0.70 for Chicys and CHIMerc, respectively) for the entire adsorption process. The plot can be divided into two regions, with distinct K_{ID} and C constants indicating that the adsorption of MO onto scaffolds occurred in stages. Moreover, the plot of $q(t)$ vs. $t^{0.5}$ did not pass through the origin ($C >> 0$, C_1 = 2.45 and C_2 = 2.21) indicating that intraparticle diffusion played a role in the adsorption process, mainly in 120 min (Chicys, C_1 = 2.45 and R^2 = 0.993), which can be attributed to the formation of the first monolayer, followed by a multilayer as time progressed, although it does not control the adsorption process [22].